2016

Performance Testing of a Vapor Injection Scroll Compressor with R407C

Thomas W. Moesch
Institut fuer Energietechnik Bitzer-Stiftungsprofessur fuer Kaelte-, Kryo- und Kompressorentechnik, Technische Universität Dresden, Germany, thomas.moesch@tu-dresden.de

Ammar M. Bahman
Ray W. Herrick Laboratories, Purdue University, United States of America, abahman@purdue.edu

Eckhard A. Groll
Ray W. Herrick Laboratories, Purdue University, United States of America, groll@purdue.edu

Performance Testing of a Vapor Injection Scroll Compressor with R407C

Thomas W. MOESCH[1], Ammar M. BAHMAN[2*], Eckhard A. GROLL[2]

[1]Technische Universitaet Dresden, Institut fuer Energietechnik,
Bitzer-Stiftungsprofessur fuer Kaelte-, Kryo- und Kompressorentechnik,
Dresden, Germany
thomas.moesch@tu-dresden.de

[2]Purdue University,
School of Mechanical Engineering,
Ray W. Herrick Laboratories,
West Lafayette, Indiana, USA
abahman@purdue.edu, groll@purdue.edu

* Corresponding Author

ABSTRACT

Current studies indicate that the method of economized vapor injection (EVI) increases both cooling capacity and coefficient of performance (COP) of vapor compression systems and enlarges the operating range of compressors by reducing the discharge temperature. The design and analysis of EVI systems require comprehensive and comparable performance data of the compressor. In this work, a thermodynamic model was developed to simulate the potential benefit of EVI systems. Furthermore, the performance of a vapor injection (VI) scroll compressor has been experimentally investigated using a modified compressor calorimeter and the refrigerant mixture R407C. During the experiments, the injection flow was regulated by controlling the injection superheat. The experimental results confirm the predicted tendencies of the EVI model. The investigation also reveals that the injection pressure affects the VI compressor performance and needs to be included in the compressor performance evaluation.

1 INTRODUCTION

The application of lubricated compressors in single-stage vapor compression cycles is limited by the pressure ratio of condensing to evaporating pressures. The main limitation is hereby the maximum compressor discharge temperature at which the lubricant starts to degrade. This limited operating envelope can be extended by refrigerant injection. Dutta *et al.* (2001) showed that using a scroll compressor and injecting liquid refrigerant into the compression pocket reduces the discharge temperature linearly with 1.5 K per percent of injection ratio, which is defined as the ratio of the injection mass flow rate to the mass flow rate through the evaporator. They found that liquid refrigerant injection is not preferable thermodynamically as it reduces the compressor efficiency and thus, increases the power consumption. Winandy and Lebrun (2002) investigated the application of a VI scroll compressor in combination with an internal heat exchanger (IHX) using R22 as a refrigerant. The IHX was used as an economizer, cooling down the refrigerant leaving the condenser while evaporating the injection mass flow at injection pressure. Their experimental results of this EVI system showed that the discharge temperature can be reduced while the cooling capacity is increased, and the systems COP remains unchanged. The design of the VI scroll compressor (Perevozchikov, 2013) allowed an unchanged evaporator mass flow rate as the additional refrigerant was solely injected within the compression process. Wang *et al.* (2009) optimized the EVI process using a detailed VI compressor model for R22. Their investigation revealed that for a fixed injection port location there is an optimal injection pressure for maximizing the cooling capacity based on given condensing and evaporating conditions. Several manufacturers already introduced VI compressors suggesting EVI cycle designs and controls (Emerson, 2015). However, the performance evaluation of VI compressors is not yet standardized. Navarro *et al.* (2013) systematically investigated the performance of a VI scroll compressor using a test setup with IHXs and the

refrigerant mixture R407C. The investigation included a variation of the injection pressure for different evaporating and condensing pressures. Their results show a dependence of the heating capacity and heating COP improvement on the intermediate pressure.

This paper presents an experimental investigation of a VI scroll compressor for a HVAC application in high temperature regions using R407C as a refrigerant. Prior to any performance tests, the operational limits of the test setup and the compressor were estimated using a thermodynamic cycle model. The experimental investigation includes performance tests with and without vapor injection and for different injection pressures.

2 EXPERIMENTAL SETUP

A VI scroll compressor with a volumetric flow rate of 14.1 m³/h was tested on an existing compressor calorimeter, which was modified for refrigerant injection as shown in Figure 1. During the test operation, the condensing pressure p_C, the evaporating pressure p_E, the return gas temperature T_{RG}, the compressor ambient air temperature T_{amb}, and the injecting superheat $\Delta T_{SH,inj}$ were adjustable. The condensing pressure was adjusted by PID-1, a PID controller which controlled the process water flow through the shell-and-tube condenser by setting the opening of valve V3 in the process water return line (PWR). The evaporating pressure was adjusted manually by changing the opening of the pneumatically driven expansion valves V1 and V1' at the inlet of the evaporators. Both evaporators sit in a secondary calorimeter filled with R134a as a secondary refrigerant. The return gas temperature was adjusted by PID-3 which controlled a 3 kW on-off heating element in the secondary calorimeter. In addition, three 3 kW and one 6 kW on-off heating elements in the secondary calorimeter were controlled manually. This allowed a wide range of cooling capacities during the compressor testing. The ambient air temperature in the compressor chamber is adjusted by PID-2 which controlled the chamber heater. The control of the injection flow was performed with an electronic expansion valve (EXV). The EXV control was based on the injection superheat which resulted from the temperature and pressure measurement at the injection port. All temperatures were measured with T-type thermocouples. The pressure measurements were conducted with absolute and gauge capacitance pressure transducers. The specifications of all measurement devices are listed in Table 1. The mass flow measurement was confirmed using the secondary calorimeter method according to ANSI/ASHRAE Standard 41.9 (2011).

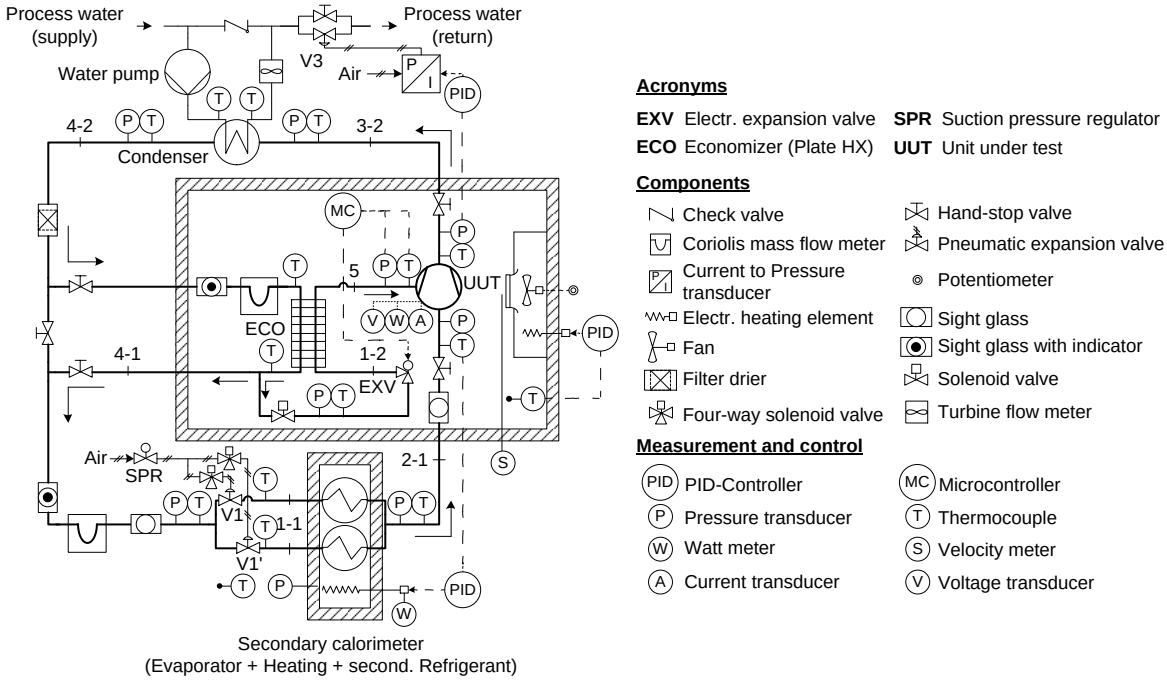

Figure 1: Sketch of modified compressor calorimeter

Table 1: Measurement devices of the test setup

Measurement	Device (Manufacturer, Model)	Accuracy
Current (compr.)	Current transducer (SC[1], 4044-8)	±0.15 % ±0.05 A
Flow rate (Evap.)	Coriolis mass flow meter (MM[2], DS040 & RFT9712)	±0.2 % ±0.24 kg/h
Flow rate (Total)	Coriolis mass flow meter (MM[2], DH025S & IFT9701)	±0.15 % ±0.18 kg/h
Flow rate (H_2O)	Turbine flow meter (EG&G, FT12)	±0.25 %
Power (compr.)	Watt/Watthour transducer (SC[1], DL31K5)	±0.09 % ±2.0 W
Power (Sec. Cal.)	Watt/Watthour transducer (SC[1], DL5C5)	±0.09 % ±1.8 W
Pressure (amb.)	Barom. pressure transducer (Setra, 278)	±0.6 mbar
Pressure (low/Sec.Cal./high)	Absolute pressure transducer (Setra, 204-100/500/1000)	±0.76 / ±3.79 / ±7.58 kPa
Pressure (eco)	Gauge pressure transducer (Setra, 207-500)	±4.48 kPa
Temperature	Thermocouples (Omega, T)	±1 K
Velocity (air amb.)	Air velocity transmitter (Dwyer, 640-1)	±2 %
Voltage (compr.)	Voltage transducer (SC[1], 3588)	±0.25 %

1) Science Columbus, 2) Micro Motion

3 THERMODYNAMIC MODEL

3.1 Model Parameters

The modified calorimeter model is based on an ideal vapor compression cycle and a supplementary refrigerant injection circuit with an IHX economizer as shown in Figure 2. The refrigerant is extracted downstream after the economizer. The calculation of the models state points (SP) requires nine parameters. The main cycle parameters such as the saturated condensing/evaporating temperature $T_{dew,C}/T_{dew,E}$, the high pressure subcooling ΔT_{SC}, and the low pressure superheat ΔT_{SH} resemble the operating conditions of regular compressor performance tests. The supplementary circuit is defined by the injection pressure superheat $\Delta T_{SH,inj}$ and the minimal temperature difference at the economizer ΔT_{min}. The compressor model is reduced to three parameters, the overall isentropic efficiency ε_c, the volumetric efficiency ε_v and the theoretical volume displacement $\dot{V}_{th}$ .The volumetric efficiency includes the effect of inner leakages and the internal heat flux to the suction volume flow. The overall isentropic efficiency describes the irreversibility of the compression process. The theoretical volume displacement was the only geometric compressor parameter and given by the manufacturer.

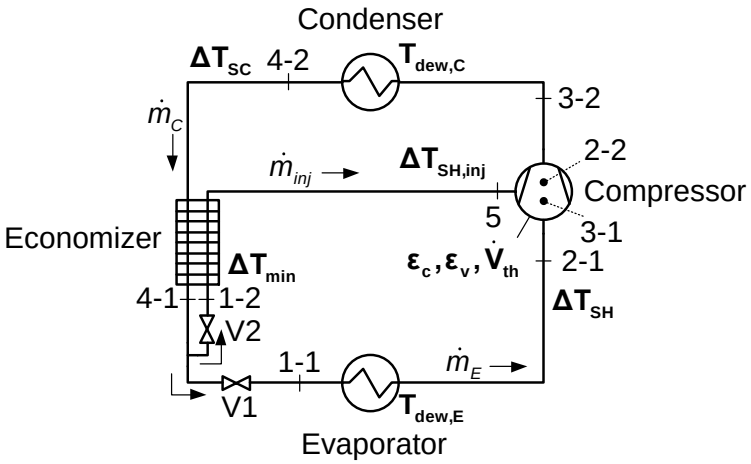

Figure 2: Parameters for EVI cycle model

3.2 Cycle Analysis

The analysis of the thermodynamic model excluded any internal pressure losses that are not associated with the expansion devices, or any external heat losses that are not associated with the heat exchangers. Further, the composition of the refrigerant mixture was assumed to be the same at all SP and the circulation of lubricant was not considered. The EVI system operates at three different pressures levels: the condensing pressure p_C, the evaporating pressure p_E, and the injection pressure p_{inj}. The pressures were derived from their saturated temperatures as stated in Equation (1).

$$p_{C/E/inj} = p_{dew}\left(T_{dew,C/E/inj}\right) \tag{1}$$

The saturated injection temperature $T_{dew,inj}$ was estimated using Equation (2). This empirical correlation was given by Emerson (2015) as part of the economizer sizing process for their VI scroll compressors. The correlation is valid for condensing temperatures $T_{dew,C}$ = 26.6 to 65.6 °C and evaporating temperatures $T_{dew,E}$ = -31.6 to 10.0 °C, and it was based on the assumption of fixed temperature differences $\Delta T_{min} = \Delta T_{SC} = \Delta T_{SH}$ = 5.6 K. The claimed accuracy of this correlation is ± 2.8 K.

$$T_{dew,inj} = 0.8 \cdot T_{dew,E} + 0.5 \cdot T_{dew,C} - \frac{19}{3}\mathrm{K} \tag{2}$$

The total mass flow rate through the condenser is divided at the economizer outlet (SP 4-1) which yields to the mass conservation as stated in Equation (3). The mass flow rate through the evaporator was calculated using Equation (4) which is based on the definition of the volumetric efficiency. The energy conservation of the economizer and the assumption of an isenthalpic expansion across V2 yields to the injection ratio μ_{inj} as stated in Equation (5).

$$\dot{m}_C = \dot{m}_E + \dot{m}_{inj} = \dot{m}_E \cdot \left(1 + \mu_{inj}\right) \tag{3}$$

$$\dot{m}_E = \varepsilon_v \cdot \frac{\dot{V}_{th}}{v_{2-1}} = \varepsilon_v \cdot \frac{\dot{V}_{th}}{v\left(p_E, T_{dew,E} + \Delta T_{SH}\right)} \tag{4}$$

$$\mu_{inj} = \frac{\dot{m}_{inj}}{\dot{m}_E} = \frac{\Delta h_{SC,eco}}{h_5 - h_{4-2}} = \frac{\Delta h_{SC,eco}}{h\left(p_{inj}, T_{dew,inj} + \Delta T_{SH,inj}\right) - h\left(p_C, T_{bub,C} - \Delta T_{SC}\right)} \tag{5}$$

Where $T_{bub,C} = T_{bub}(p_C)$ is the bubble point temperature at condensing pressure and $\Delta h_{SC,eco}$ is the specific enthalpy difference that represents the additional subcooling in the liquid line of the economizer as stated in Equation (6). The temperature T_{4-1} is determined iteratively using Equation (7), which assumes an isenthalpic expansion across V2 and includes the constraint ΔT_{min} at the economizer outlet.

$$\Delta h_{SC,eco} = h_{4-2} - h_{4-1} = h\left(p_C, T_{bub,C} - \Delta T_{SC}\right) - h\left(p_C, T_{4-1}\right) \tag{6}$$

$$h\left(p_C, T_{4-1}\right) = \begin{cases} h\left(p_{inj}, T_{4-1} - \Delta T_{min}\right) & \text{when } \mu_{inj} > 0 \\ h_{4-2} & \text{when } \mu_{inj} = 0 \end{cases} \tag{7}$$

The cooling capacity $\dot{Q}_E$ is defined by the enthalpy difference across the evaporator as stated in Equation (8). The assumption of an isenthalpic expansion across V1 and the additional subcooling $\Delta h_{SC,eco}$ yield to Equation (9).

$$\dot{Q}_E = \dot{m}_E \cdot \left(h_{2-1} - h_{1-1}\right) \tag{8}$$

$$\dot{Q}_E = \dot{m}_E \cdot \left(h_{2-1} - h_{4-2} + \Delta h_{SC,eco}\right) = \dot{m}_E \cdot \left[h\left(p_E, T_{dew,E} + \Delta T_{SH}\right) - h\left(p_C, T_{bub,C} - \Delta T_{SC}\right) + \Delta h_{SC,eco}\right] \tag{9}$$

The compression process in this model was divided in a pre-injection compression (SP 2-1 to 3-1) and a post-injection compression (SP 2-2 to 3-2). The pre-injection compression as stated in Equation (10) is assumed to end at the injection pressure whereas the post-injection compression as stated in Equation (11) starts at the injection pressure. The injection process was simplified to an adiabatic and isobaric mixing process at injection pressure and results in the mixing enthalpy $h_{2\text{-}2(s)}$ as stated in Equation (12).

$$h_{3-1} = \frac{h_{3-1s} - h_{2-1}}{\varepsilon_c} + h_{2-1} = \frac{h\left(p_{inj}, s_{2-1}\right) - h\left(p_E, T_{dew,E} + \Delta T_{SH}\right)}{\varepsilon_c} + h\left(p_E, T_{dew,E} + \Delta T_{SH}\right) \tag{10}$$

$$h_{3-2} = \frac{h_{3-2s} - h_{2-2s}}{\varepsilon_c} + h_{2-2} = \frac{h\left(p_C, s_{2-2s}\right) - h_{2-2s}}{\varepsilon_c} + h_{2-2} \tag{11}$$

$$h_{2-2(s)} = \frac{\dot{m}_E \cdot h_{3-1(s)} + \dot{m}_{inj} \cdot h_5}{\dot{m}_E + \dot{m}_{inj}} = \frac{h_{3-1(s)} + \mu_{inj} \cdot h_5}{1 + \mu_{inj}} \tag{12}$$

The compressor discharge temperature was calculated using the specific enthalpy $h_{3\text{-}2}$ at the end of the post-injection compression. The compressor power consumption was calculated as stated in Equation (14), which results from Equations (10) to (12).

$$T_{dis} = T_{3-2} = T\left(p_C, h_{3-2}\right) \tag{13}$$

$$P_{comp} = \left(\dot{m}_E + \dot{m}_{inj}\right) \cdot \left(h_{3-2} - h_{2-2}\right) + \dot{m}_E \left(h_{3-1} - h_{2-1}\right) = \dot{m}_E \cdot \frac{\left(1 + \mu_{inj}\right) \cdot h_{3-2s} - \mu_{inj} \cdot h_5 - h_{2-1}}{\varepsilon_c} \tag{14}$$

The software REFPROP (Lemmon *et al.*, 2013) was used to calculate the refrigerant's thermodynamic properties such as the saturated pressures $p_{dew/bub}(T)$, the saturated temperatures $T_{dew/bub}(p)$, the specific volume $v = v(p,T)$, the specific enthalpy $h = h(p,T)$, and the specific entropy $s = s(p,T)$.

3.3 Performance Test Simulation

The model was used to conduct simulations for two different compressor operating conditions, the baseline (BL) operation with $\mu_{inj} = 0$ and the vapor injection (VI) operation with $\mu_{inj} > 0$. For the simulation, $T_{dew,C}$ and $T_{dew,E}$ were varied and the remaining parameters were kept constant as stated in Table 2. The results lead to the definition of a limited test envelope for the BL and VI operation as shown in Figure 3A. The envelope boundaries were based on the limits for both calorimeter and compressor. The restricting parameter for the given calorimeter was the cooling capacity, which was limited to a range of 5 kW to 15 kW. The operation of the scroll compressor was limited to $T_{dis,max} = 115$ °C and $I_{max} = 18$ A. The maximum compressor power consumption resulted from Equation (15), which assumes a symmetric power distribution for a three phase power supply. This lead to a maximum power consumption $P_{comp,max} = 6.095$ kW for a power factor $\cos(\varphi) = 0.85$ at $U_{comp} = 230$ V.

$$P_{comp,max} = \cos\left(\varphi\right) \cdot \sqrt{3} \cdot I_{max} \cdot U_{comp} \tag{15}$$

The simulation reveals the benefits of the EVI system on the compressor performance. The operating envelope expands towards higher compression ratios through the reduction of the discharge temperature, and the cooling capacity is raised. However, the simulation results also show the impact of the calorimeter limitation, which reduces the amount of possible test points for evaporating temperatures past 4.5 °C.

Table 2: Parameter assumption for the performance test simulation

ΔT_{SH}	ΔT_{SC}	$\Delta T_{SH,inj}$	ΔT_{min}	ε_c	ε_v	$\dot{V}_{th}$
11.11 K	5.56 K	5.56 K	5.56 K	0.7	0.9	14.1 m³/h

4 PERFORMANCE TESTS AND RESULTS

4.1 Test Conditions

Similar to the simulation, the experiment was conducted for two different kinds of compressor operating conditions. During BL operation, the injection port of the scroll compressor was closed and the EVI circuit was bypassed. All steady state test points of the BL operation are plotted in Figure 3A, which also shows the calculated test limits. During VI operation the injection port was opened and the bypass of the EVI circuit was closed. The VI test points were based on two BL conditions at different injection conditions as shown in Figure 3A and Figure 3B. During Condition A ($T_{dew,C}$ = 48.9 °C, $T_{dew,E}$ = 4.5 °C) the impact of two-phase injection was investigated by changing the opening of the EXV between 10 to 30 %. The influence of elevated condensing temperatures on the EVI performance was investigated at Condition B ($T_{dew,C}$ = 60.0 °C, $T_{dew,E}$ = 4.5 °C) while the injection superheat was varied from 0 to 34.6 K. All compressor performance tests were conducted for a suction superheat of 11.1 K and an ambient compressor temperature of 35 °C. During each test condition, the refrigerant charge remained constant, which caused a variation in the subcooling at the condenser outlet (SP 4-2). Depending on the evaporating and condensing conditions, the subcooling varied between 0.5 K and 4.3 K for the BL operation and between 2.3 K and 4.9 K for the VI operation.

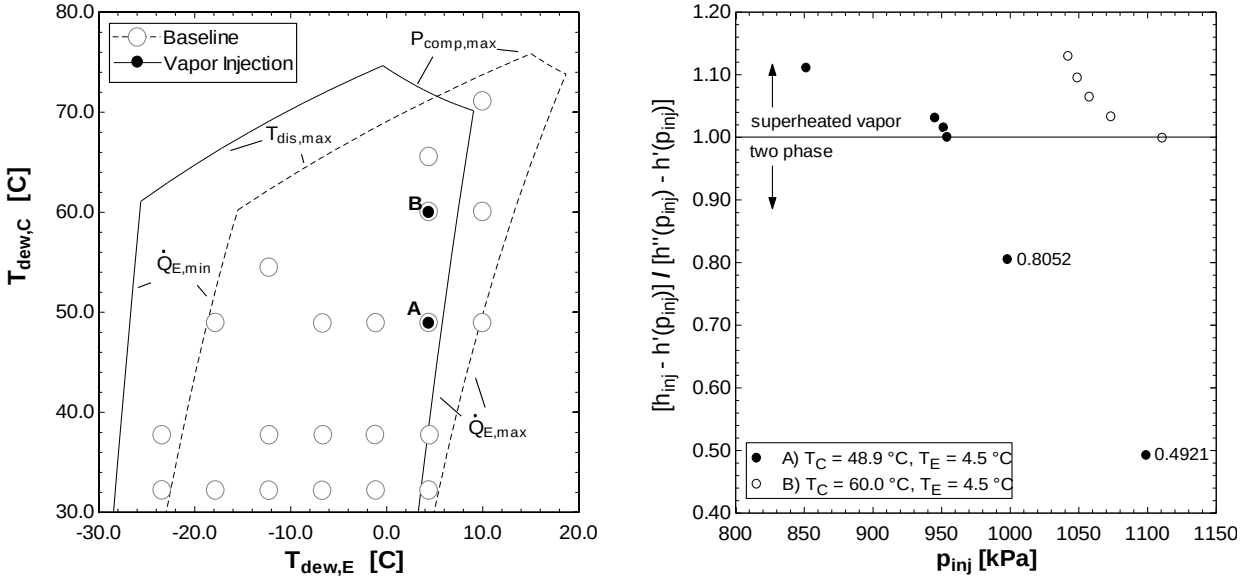

A) Test conditions for BL and VI tests

B) Injection conditions during VI tests

Figure 3: Test matrix for performance tests

4.2 Baseline Test Results and Analysis

The results of the baseline performance tests are illustrated in Figure 4A through 4D. The cooling capacity decreased towards increased pressure ratios and ranges from 4 to 15.5 kW as shown in Figure 4A. This was caused by two effects, the reduction of the suction mass flow rate for lower evaporating temperatures and the reduction of the specific enthalpy difference across the evaporator for increased condensing temperatures. The trend of the cooling capacity is in good agreement with the simulation results. The error of ±7% can be explained with the lack of subcooling. The trend of the discharge temperature is shown in Figure 4B. It increased for growing compression ratios reaching values up to 113 °C. The error of the simulated discharge temperature was up to ±10 K for lower evaporating temperatures. This was mainly caused by the decreasing efficiency as illustrated in Figure 4C. The trend of ε_c results from the built-in volume ratio of the scroll compressor. According to Winandy *et al.* (2002), the isentropic efficiency reaches its maximum for an adapted compression ratio and decreases for any external pressure ratio that differs from the inner ratio. By analyzing the trend of the compressor efficiency, the adapted pressure ratio was estimated to be 3.65. The volumetric efficiency of this scroll compressor ranged from 0.86 to 0.96. This rather high ε_v is common for scroll compressors, which generally lack any dead volume and do not encounter re-expansion

after the compression process. The reduction of the volumetric efficiency, as shown in Figure 4D, results from increased internal leakages and additional motor losses, which increase the internal suction temperature.

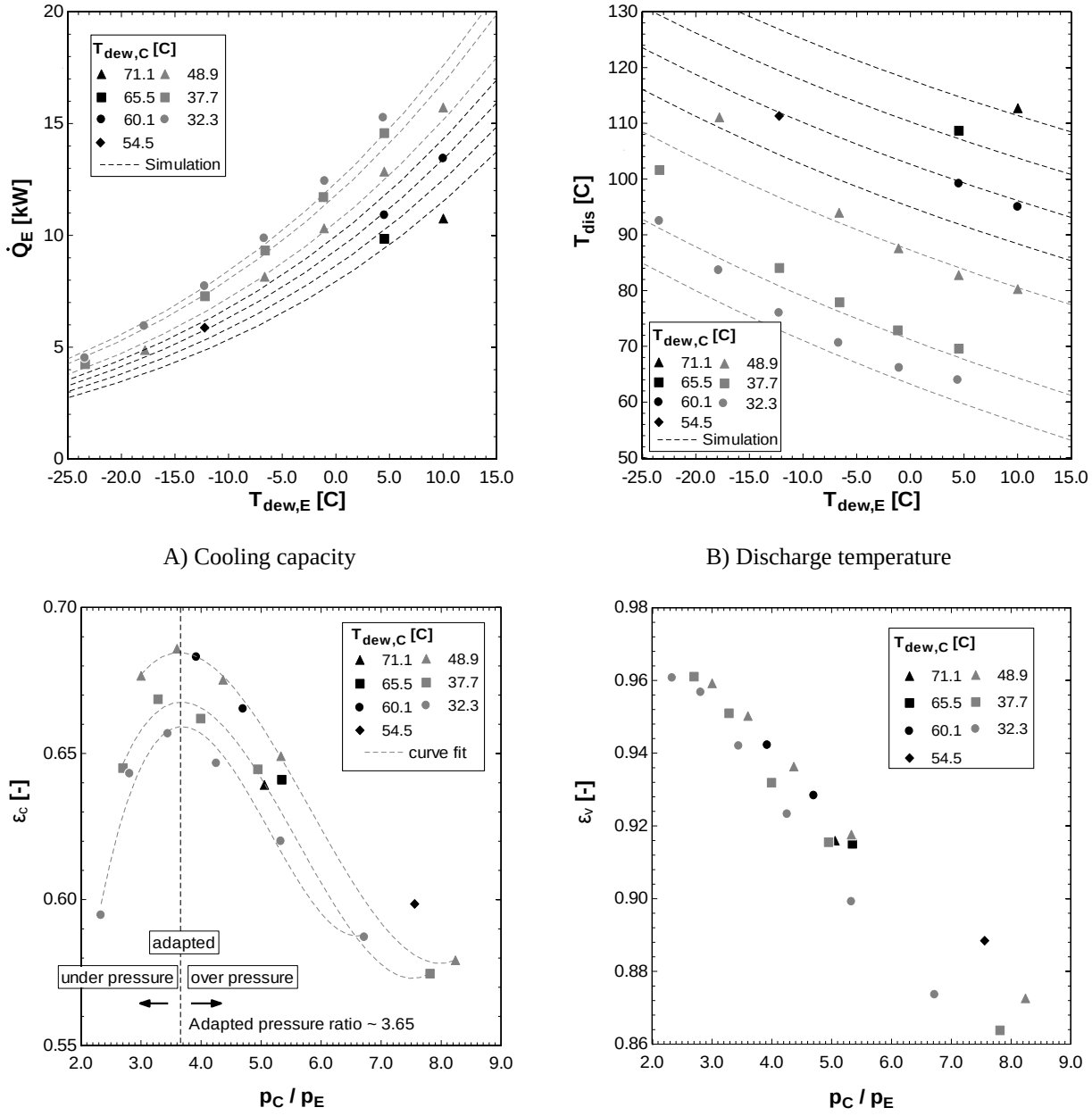

A) Cooling capacity

B) Discharge temperature

C) Overall isentropic efficiency

D) Volumetric efficiency

Figure 4: Performance values during baseline operation

4.3 Vapor Injection Test Results and Analysis

The results of the vapor injection performance tests for the Operating Conditions A and B are illustrated in Figure 5A through 5D. The cooling capacity was raised by 12 to 30% compared to the baseline tests. For vapor injection, the cooling capacity increased with increasing injection pressure until two phase-injection started. The decrease in cooling capacity for wet injection can be explained with an increased saturated temperature on the cool side of the economizer which leads to a reduced subcooling of the liquid refrigerant. The optimum injection pressure for maximum cooling capacity as described by Wang *et al.* (2009) was found to be 94% of the geometric mean of

evaporating and condensing pressure at the given conditions. The simulation underestimated the cooling capacity by up to 5%. This underestimation was mainly caused by the assumption of ΔT_{min}, which reached values of 0.4 to 4 K during the VI performance tests. The discharge temperature generally decreased with increased injection pressures. For the two tested conditions, the rate of reduction was found to be dependent on the phase of the injected refrigerant and the condensing temperature as shown in Figure 5B. For Operating Condition A, the reduction rate increased from -3.5 K to -13.1 K per 100 kPa when the injection changed to two-phase injection. During two-phase injection the latent heat of the injected refrigerant causes extra cooling. Compared to Operating Condition A, the reduction during Operating Condition B was more effective with a rate of -9.7 K/100 kPa. This was due to the higher injection pressure, which increased the injection mass flow rate and thus, reduced the mixing temperature after injection. During the VI operation, P_{comp} increased linearly with the injection pressure as shown in Figure 5C. The rate was approximately 204 W/100 kPa for both operating conditions. This leads to an increase in the power consumption of 7.5 to 22.5% compared to the BL operation. The simulation model underestimated the power consumption by 12.5%. The reason for this error is the isentropic compressor efficiency, which was lower than the assumed value of 0.7. Figure 5D shows the reduction of ε_c for increasing injection pressures. For vapor injection the isentropic compressor efficiency decreased by only 0.01 / 100 kPa. However, when the injection turned into wet injection, this rate changed to 0.05 / 100 kPa. During VI operation, ε_c was decreased by -5% to -16.8% compared to the BL operation. The volumetric efficiency remained constant during VI within a range of ±0.005. Compared to BL operation, ε_v was reduced by -3%. The reason for this reduction could be an increase in internal leakages during injection.

5 CONCLUSIONS

A VI scroll compressor has been successfully tested on a modified compressor calorimeter at high temperature range using R407C. The thermodynamic model presented in this paper allowed the creation of a limited test envelope for the performance test of a given compressor. The experimental results indicated that the injection pressure had a significant impact on the performance of the VI compressor. The VI compressor was characterized in regard to its adapted pressure ratio and optimized injection pressure. It was found that the reduction rate of the discharge temperature depends on the phase of the injected refrigerant and the condensing temperature. Further, this paper reveals that any injection pressure might degrade the isentropic and volumetric efficiency of the given compressor compared to an operation without vapor injection. Since the injection pressure influences the degree of the discharge temperature reduction, the cooling capacity improvement, and the isentropic compressor efficiency, their values and variations should be included in future compressor performance tests.

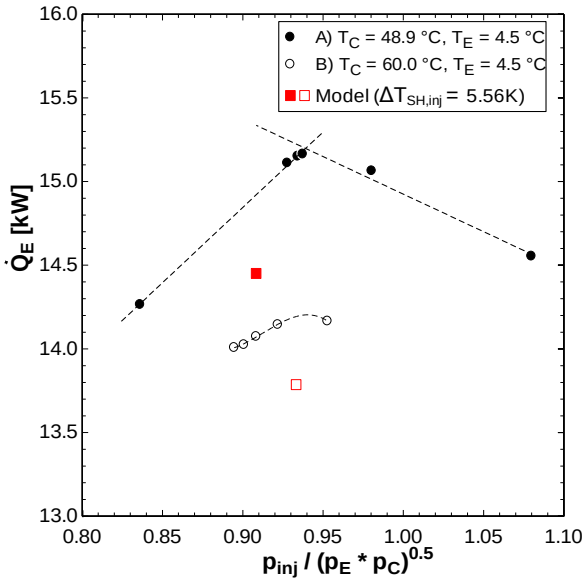

A) Cooling capacity

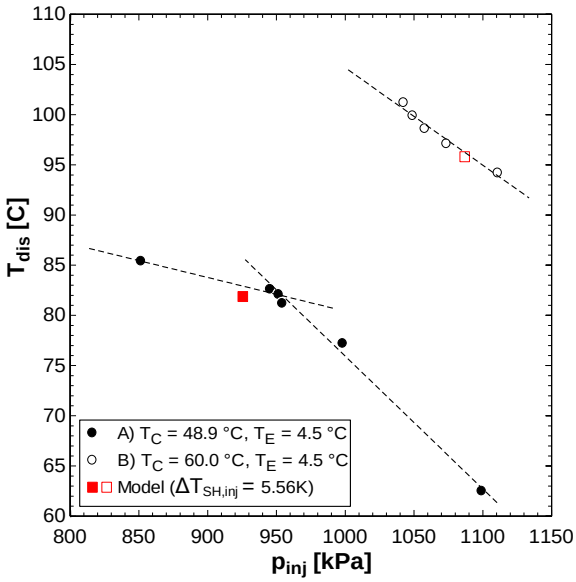

B) Discharge temperature

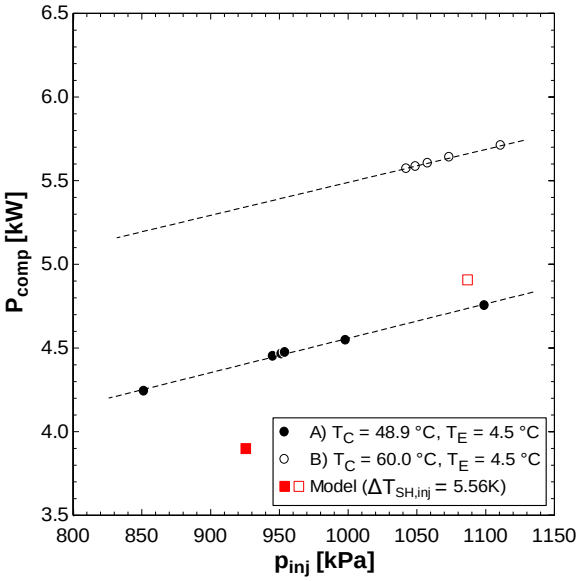

C) Power consumption

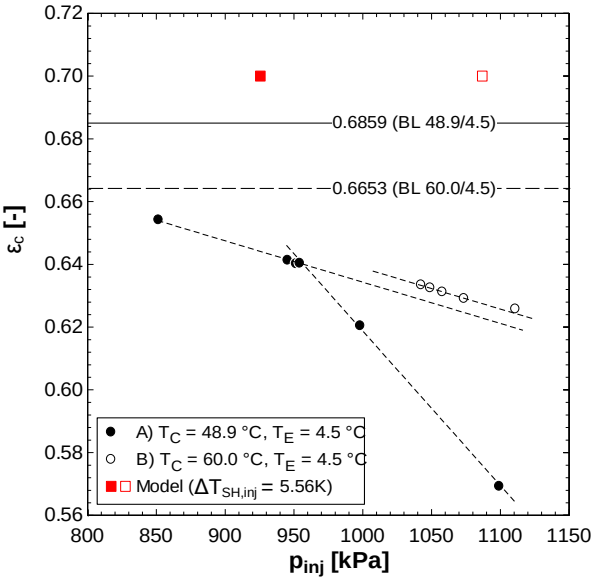

D) Overall isentropic efficiency

Figure 5: Performance values during vapor injection operation

NOMENCLATURE

COP	Coefficient of performance	(-)	eco	Economizer
h	Specific enthalpy	(kJ/kg)	inj	Injection
$\dot{m}$	Mass flow rate	(kg/h)	min	Minimum
p	Pressure	(kPa)	s	Isentropic
$\dot{Q}$	Capacity	(W)	SC	Subcooling
s	Specific entropy	(kJ/kgK)	SH	Superheat
T	Temperature	(°C)	th	Theoretical
v	Specific volume	(m^3/kg)	**Superscripts**	
$\dot{V}$	Volume flow rate	(m^3/h)	'	Bubble point
Greek			"	Dew point
Δ	Difference	(-)	**Acronyms**	
ε_c	Overall isentr. compr. efficiency	(-)	BL	Baseline
ε_v	Volumetrtic efficiency	(-)	EVI	Economized Vapor Injection
μ	Mass flow ratio	(-)	EXV	Electronic Expansion Valve
Subscripts			IHX	Internal heat exchanger
1-1...4-2, 5	State points		PID	Proportional, integration, Differential
bub	Bubble point			
C	Condensing		PWR	Process water return
comp	Compressor		Sec. Cal.	Secondary calorimeter
dew	Dew point		SP	State point
dis	Discharge		VI	Vapor Injection
E	Evaporating			

REFERENCES

ANSI/ASHRAE Standard 41.9-2011, *Standard methods for volatile-refrigerant mass flow measurements using calorimeters*, American Society of Heating, Refrigerating and Air-Conditioning Engineers, Inc., 1791 Tullie Circle NE, Atlanta, GA 30329.

Dutta, A.K., Yanagisawa, T., Fukuta, M., 2001, An investigation of the performance of a scroll compressor under liquid refrigerant injection, *Int. J. Refrig.*, vol. 24, no. 6, p. 577-587.

Emerson Climate Technologies (Ed.), 2015, Economized Vapor Injection (EVI) Compressors, *Bulletin AE4-1327 R12*. Emerson Climate Technologies, Inc., 22p.

Lemmon, E.W., Huber, M.I., McLinden, M.O., 2013, NIST Standard Reference Database 23: Reference Fluid Thermodynamic and Transport Properties (RefProp), Version 9.1, National Institute of Standards and Technology, Standard Reference Data Program, Gaithersburg.

Navarro, E., Redón, A., Gonzálvez-Macia, J., Martinez-Galvan, I.O., Corberán, J.M., 2013, Characterization of a vapor injection scroll compressor as a function of low, intermediate and high pressures and temperature conditions, *Int. J. Refrig.*, vol. 36, no. 7, p. 1821-1829.

Perevozchikov, M.M., 2003, Scroll compressor with vapor injection, U.S. Patent, No. 0133819.

Wang, B., Shi, W., Han, L., Li, X., 2009, Optimization of refrigeration system with gas-injected scroll compressor, *Int. J. Refrig.*, vol. 32, no. 7, p. 1544-1554.

Winandy, E., Saavedra, C., Lebrun, L., 2002, Experimental analysis and simplified modeling of a hermetic scroll refrigeration compressor, *Applied Thermal Engineering*, vol. 22, no. 2, p. 107-120.

Winandy, E.L., Lebrun, J., 2002, Scroll compressors using gas and liquid injection: experimental analysis and modeling, *Int. J. Refrig.*, vol. 25, no. 8, p. 1143-1156.